Comprehensive Efficiency Analysis of Current Source Inverter Based SPM Machine Drive System for Traction Applications

Feida Chen Wenda Feng Hao Ding Sangwhee Lee Thomas M. Jahns Bulent Sarlioglu
Wisconsin Electric Machines and Power Electronics Consortium (WEMPEC)
Department of Electrical and Computer Engineering
University of Wisconsin-Madison, WI 53706 USA
E-mail: sarlioglu@wisc.edu

***Abstract*—A current-source inverter (CSI) has the natural capability of boosting the output voltage which is a notable advantage over voltage source inverter (VSI) in traction drive applications. This paper investigates the voltage boosting feature of the CSI to improve the overall efficiency of the CSI-based surface permanent magnet (SPM) machine drive system in the constant power region. The effects of the boost function on the total system losses, including the machine copper loss, core loss, and magnet loss, as well as the device conduction and switching loss in the CSI and dc/dc converter, are described using analytical models. The operating characteristics of the machine and CSI are validated by 2-D finite-element analysis (FEA) and simulations. Based on the loss model, the effects of the modulation index on the overall drive system losses and power factor have been analyzed. A genetic algorithm has been used to optimize the CSI's boost ratio, demonstrating that the drive system efficiency can be increased by 1% to 2.5% along the constant-power regime envelope by using the boost function.**

Keywords—current source inverter, genetic algorithm, SPM machine, system loss, traction application, voltage boost function

I. Introduction

Electric vehicles (EVs) have been rapidly developed for transportation applications during the past decade due to their reductions of fuel usage and greenhouse emissions [1,2]. The efficiency of the traction system is very important to reduce its thermal stress and extend the vehicle range [3]. The copper loss is one of the dominant components among the machine losses for a given machine design, which is proportional to the square of the stator current amplitude. The current-source inverter (CSI) has the natural capability of boosting the voltage and reducing the current in the constant power region, which can be beneficial for motor efficiency. However, the boost function reduces the efficiency of the CSI because the high output voltage increases the switching loss. Therefore, an investigation of the total drive system efficiency instead of focusing on the machine or inverter efficiency alone is necessary to fairly evaluate the CSI's potential benefits.

A CSI-based traction drive configuration is shown in Fig.1. The traction drive includes a battery, a bi-directional dc/dc converter, a CSI, and an SPM machine. The bi-directional dc/dc converter converts the voltage source (battery) into a regulated current source supplying the CSI, and it enables the CSI to charge the battery during braking operation of the machine [4].

The CSI replaces the VSI's dc-link capacitor with a dc-link inductor and three small output capacitors which provides more sinusoidal output voltage waveforms to the machine and lower common-mode EMI emissions compared to the voltage-source inverter (VSI) [5]. Dai, *et al* have demonstrated that the CSI offers valuable performance advantages over the baseline VSI by using wide-bandgap (WBG) power switches [5,6]. Su, *et al* compare the power loss of the CSI and VSI for traction drive application [7]. The boost function of CSI to extend constant-torque and constant-power speed range is investigated for EVs application in [8,9]. However, few researchers have investigated the system efficiency improvement available from the CSI's voltage boost capability. Furthermore, the existing efficiency optimization analyses are mostly focused on the machine's efficiency improvement [9, 10], and the inverter losses are typically not included in the optimizations. Some machine drive system efficiency optimization methods have been applied to VSIs by searching for the optimal direct-axis current (I_d) and switching frequency [2, 3]. However, there is a knowledge gap regarding the opportunity for drive system efficiency improvement by taking advantage of the CSI's boost function.

This paper investigates the benefits of the CSI voltage boost function for drive system loss reduction and proposes a multi-objective optimization using genetic algorithm to improve the performance of the drive system. In Section II, the voltage-boost feature of the CSI is investigated, and the SPM machine is

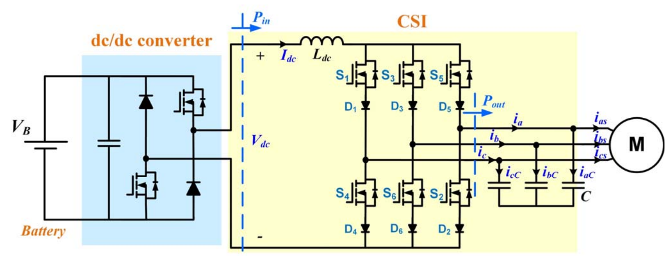

Fig. 1. CSI-based machine drive system for traction application including bidirectional dc/dc voltage-to-current source front-end converter.

modeled including consideration of the CSI's ac capacitors. In Section III, a CSI-based SPM machine design with a high constant power speed ratio (CPSR) is presented. In Section IV, the SPM machine losses, CSI losses, and dc/dc converter losses are modeled. In Section V, the power losses of the machine, CSI, and dc/dc converter are evaluated using JMAG and PLECS. Section VI discusses the impact of the modulation index on the power losses and proposes an efficiency optimization strategy based on the genetic algorithm. Conclusions are presented in the last section.

II. VOLTAGE BOOST FUNCTION OF CSI

A notable advantage of the CSI over VSI in traction drive applications is the CSI's natural output voltage boost function [10]. While the theoretical peak line-to-line voltage of the VSI is limited to the dc-link voltage V_{dc} by using a space vector pulse width modulation (SVPWM) algorithm, the CSI can deliver higher output voltage due to its boost characteristics. When the two switches in a single CSI phase leg are turned on at the same time, there is no output terminal current flowing into the filter capacitor or the machine load. Instead, this condition creates a short-circuit state (zero vector) to charge the dc-link inductor, increasing the inductor current. After the CSI switches to an active current state, the inductor current charges (or discharges) the capacitors which makes it possible to boost the applied machine voltage, reflecting the CSI's voltage boost capability.

Assuming that the CSI delivers sinusoidal output voltage and current waveforms, which can be a good approximation using wide band-gap switches [5], the steady-state CSI input and output power relationships can be presented as:

$$P_{in\_CSI} = V_{dc} \cdot I_{dc} \tag{1}$$

$$P_{out\_CSI} = \sqrt{3} V_{llpk} I_{pk} cos(\theta + \varphi)/2 \tag{2}$$

where P_{in_CSI} and P_{out_CSI} are the input power and output power of CSI, respectively; V_{dc} and I_{dc} are the average dc-link voltage and current, respectively, measured at the input terminal of the dc-link inductor; V_{llpk} is the peak line-to-line voltage, I_{pk} is the peak CSI phase current before the capacitor, θ is the angle between the motor phase voltage and stator current after the capacitor (i.e., power factor angle), and φ is the angle between the CSI phase current (before the capacitors) and stator current.

Assuming initially that there are no power losses in the CSI ($P_{in\_CSI} = P_{out\_CSI}$), the voltage boost ratio can be expressed as

$$\frac{V_{llpk}}{V_{dc}} = \frac{2}{\sqrt{3} cos(\theta + \varphi)} \cdot \frac{1}{m} \tag{3}$$

where m is the scalar value of the CSI modulation index which is defined as

$$m = \frac{I_{pk}}{I_{dc}} \tag{4}$$

This voltage boost equation shows that it is convenient to raise the motor terminal voltage above the dc-link voltage by reducing the modulation index.

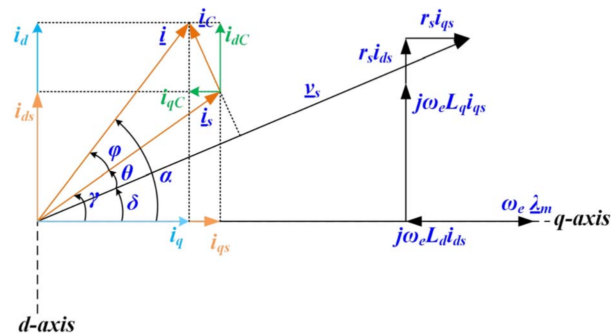

Fig. 2. Steady-state vector diagram of the CSI-based PM machine including the impact of the filter capacitors at the CSI output terminals.

To reduce the modeling error, the effect of the three small ac capacitors connected to the output terminals of the CSI cannot be ignored in the high-speed region. The vector diagram of the CSI-based motor in the rotor reference frame is presented in Fig. 2.

In Fig. 2, α is the angle between the back-EMF of the motor and CSI output current $\underline{i}$ which is the current before the capacitors; γ is the angle between the back-EMF $\omega_e \underline{\lambda}_m$ and stator current $\underline{i}_s$, which is the internal power factor angle (also known as the machine current angle); δ is the angle between the output phase voltage $\underline{v}_s$ and back-EMF known as the torque or load angle.

For steady-state operating conditions, the scalar q- and d-axis voltages and currents of the machine in the rotor reference frame are related by

$$v_{qs} = r_s i_{qs} + \omega_e L_d i_{ds} + \omega_e \lambda_m \tag{5}$$

$$v_{ds} = r_s i_{ds} - \omega_e L_q i_{qs} \tag{6}$$

where v_{qs} and v_{ds}, i_{qs} and i_{ds}, L_q and L_d are the q- and d- axis voltages, currents, and inductances of the SPM machine, respectively; r_s is the stator resistance; ω_e is the motor electrical excitation frequency; and λ_m is the magnet flux linkage.

It should be noted that the machine stator current $\underline{i}_s$ (current after the capacitors) and the CSI output current $\underline{i}$ (current before the capacitors) are different. The steady-state values of these two currents are related to each other using dq variables as follows:

$$i_{qs} = i_q - \omega_e C v_{ds} \tag{7}$$

$$i_{ds} = i_d + \omega_e C v_{qs} \tag{8}$$

where C is the capacitance of each output ac capacitor.

The relationship between the dq CSI output current variables and machine voltage variables during steady-state operation can be derived from (5), (6), (7), and (8) as:

$$\begin{aligned} v_{qs} = r_s & \frac{d \cdot i_q - a \cdot i_d + a \cdot e}{b \cdot d - a \cdot c} \\ & + \omega_e L_d \frac{c \cdot i_q - b \cdot i_d + b \cdot e}{a \cdot c - b \cdot d} \\ & + \omega_e \lambda_m \end{aligned} \tag{9}$$

$$v_{ds} = r_s \frac{c \cdot i_q - b \cdot i_d + b \cdot e}{a \cdot c - b \cdot d} - \omega_e L_q \frac{d \cdot i_q - a \cdot i_d + a \cdot e}{b \cdot d - a \cdot c} \tag{10}$$

where $a = \omega_e C r_s$,
$b = (1 - \omega_e{}^2 C L_q)$,
$c = \omega_e C r_s i_{qs}$,
$d = (1 - \omega_e{}^2 C L_d)$,
$e = (-\omega_e{}^2 C \lambda_m)$.

The steady-state CSI q- and d-axis output currents can be controlled directly by the modulation index as

$$i_q = I_{dc} \cdot m \cdot cos\alpha \tag{11}$$

$$i_d = I_{dc} \cdot m \cdot sin\alpha \tag{12}$$

In the constant-torque region, the CSI current angle α can be directly controlled to produce $i_{ds} = 0$, and the boost function is not used, which yields maximum torque per ampere (MTPA) operation for an SPM machine. In the constant-power region, the CSI current angle α (Fig. 2) is regulated to generate a flux-weakening component $i_{ds} < 0$. In addition, the value of the CSI's modulation index m can be controlled to boost the machine terminal voltage to reduce the drive system losses.

This voltage-boost feature of the CSI offers multiple advantages for a traction drive application: (a) when the battery voltage drops, the CSI can boost the output voltage to maintain the same output power; (b) the voltage boost function of the CSI can be used to extend the constant power operation region to achieve a higher CPSR than the VSI; and (c) voltage boosting can be used to improve the system efficiency while reducing the CSI's output current rating and controlling the power factor at high speed.

III. SPM Machine Design for CSI

For the conventional VSI, the output voltage is limited by the battery voltage. In contract, the CSI operates naturally as a boost-type inverter that can raise the motor terminal voltage above the dc-link voltage. Based on the higher terminal voltage compared to VSI, an SPM machine with a high CPSR of 6.25 has been designed for the CSI. The parameters and rating variables of the proposed SPM machine are shown in Table I.

This SPM machine is designed to deliver 55 kW continuous power at the corner speed of 3,200 rpm, and the maximum speed is 20,000 rpm. Concentrated windings have been adopted to raise the machine's characteristic current value sufficiently to achieve high CPSR values as well as to limit the axial length by shortening the winding end turns. The flux density distribution of the SPM machine at the rated power condition is shown in Fig. 3. The maximum lamination flux density (saturated) is 1.9 T in the stator tooth tips.

The FEA results of the torque vs. speed and power vs. speed envelope curves of the CSI-based motor drive system are shown in Fig. 4 when m = 1. The constant power operation region is

Table I. SPM Machine Design Variables and Parameters

Parameter	Value
Continuous power rating [kW]	55
Corner speed [rpm]	3,200
Maximum speed [rpm]	20,000
Rated torque @ continuous power [Nm]	167
Rated phase current @ continuous power [A_{rms}]	91.9
Rated line-neutral voltage @ cont. power [V_{rms}]	297
Stator/rotor core material	10JNHF600
Magnets	N38 NdFeB
Number of stator slots	18
Number of rotor poles	12
Current density @ Rated Power [A_{rms}/mm^2]	9.2
d-axis inductance [mH]	1.07
q-axis inductance [mH]	1.11
Phase winding resistance [Ω]	0.082
No-load magnet flux linkage λ_m [Wb_{rms}]	0.1035
Characteristic current = λ_m/L_d [A_{rms}]	96.7

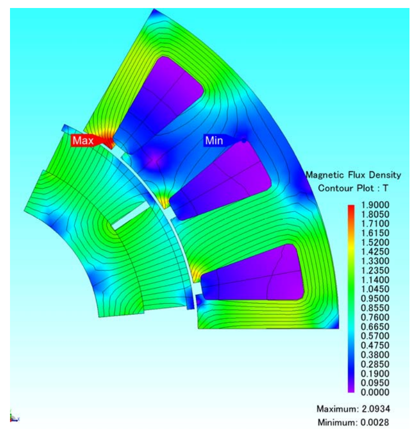

Fig. 3. 2-D FEA flux density distribution of the proposed SPM machine at rated power operation condition (55 kW, 3200 rpm).

from 3,200 rpm to 20,00 rpm. The corresponding value of the current angle γ vs. speed for these envelope curves is shown in Fig. 5. Fig. 5 shows a large negative d-axis current must be applied in the deep flux-weakening region when the modulation index is held constant at m = 1. However, when m < 1, less flux weakening current is required because the machine voltage is raised. The reduced CSI output current reduces the stator copper loss, but the boosted machine terminal voltage increases the CSI's switching loss. The optimal modulation index value to maximize efficiency is investigated in the following section.

IV. Loss Modeling of CSI-SPM Machine System

A. Loss Model of SPM Machine

The electrical loss in the SPM machine can be expressed as (13), where P_{Cu} is the copper loss in the windings, P_{Fe} is the core loss in the stator and rotor, and P_{magnet} is the permanent magnet loss.

$$P_{motor} = P_{Cu} + P_{Fe} + P_{magnet} \tag{13}$$

The copper loss is one of the dominant components among the machine losses which includes dc copper loss, skin effect

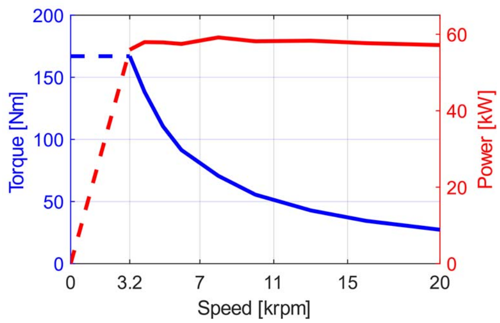

Fig. 4. FEA-based torque vs. speed and power vs. speed envelope curve of the CSI-based machine when the modulation index is held constant, $m = 1$.

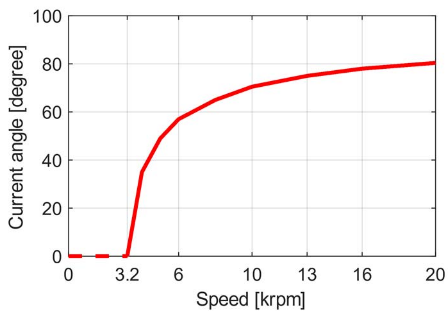

Fig. 5. FEA-based current angle γ of the SPM machine for the envelope curves in Fig. 4 when the modulation index value is held constant, $m = 1$.

loss, and proximity effect loss. To facilitate the analysis, the dc copper loss can be expressed as $I_{rms}{}^2 R_{dc}$, where I_{rms} is the rms value of the motor current and R_{dc} is the dc resistance per phase, which can be easily calculated based on the winding design details. The ac copper loss due to the skin effect and proximity effect typically cannot be ignored when operating at high speed with high fundamental frequency. The ac winding resistance is estimated as [12]

$$R_{ac} = \frac{\pi \sigma l_c r_c{}^4 \mu_0{}^2 \omega_e{}^2 N_s N_t{}^3}{12 w_{si}{}^2} \tag{14}$$

where σ is the conductivity of the wire, l_c is the wire length per turn, r_c is the conductor radius, μ_0 is the magnetic permeability of free space, ω_e is the fundamental angular frequency (rad/s) of the current, N_s is the number of slots, N_t is the number of turns per coil, and w_{si} is the width of the slot.

Using this approach, the copper loss can be evaluated as

$$P_{Cu} = 3 I_{rms}{}^2 (R_{dc} + R_{ac}) \tag{15}$$

where the rms value of the phase current of motor can be calculated as

$$I_{rms} = \sqrt{\frac{i_{qs}{}^2 + i_{ds}{}^2}{2}} \tag{16}$$

The core loss is composed of eddy current loss and hysteresis loss which is estimated using the classic Steinmetz's equation as

$$P_{core} = P_h + P_e = C_{hy} f^a B^b + C_e f^2 B^2 \tag{17}$$

where P_h and P_e are the core hysteresis loss and eddy current loss, respectively. C_{hy} is the hysteresis loss coefficient, C_e is the eddy current loss coefficient, f is the fundamental frequency of the magnetic field, and B is the amplitude of the flux density. To make the calculation simpler, it will be assumed that $a = 1$ and $b = 2$.

It should be noted that the flux vs. time is not sinusoidal because of the effects of the machine's geometry as the rotor moves past the stator and magnetic saturation. Assuming that the losses can be decomposed into harmonic components occurring at multiple harmonic frequencies, the approximate total core loss can be represented as

$$P_{fe} = \sum_{n=1}^{\infty} [C_{hy} n f B_n + C_e (nf)^2 B_n{}^2] \tag{18}$$

where B_n is the peak flux density of the nth harmonic of the base frequency f, which can be predicted through the 2-D FEA simulation.

The rotor magnets in the proposed SPM machine are assumed to be highly segmented, which significantly reduces the associated magnet loss. As a result, the segmented magnet losses are much smaller than the copper loss when the machine is operating under load. Therefore, the effect of the segmented magnet losses on the system efficiency is small enough to be ignored during the optimization.

B. Loss Model of CSI

Series-connected SiC MOSFETs and SiC Schottky diodes are used in the CSI, as shown in Fig. 1. The CSI power loss consists of the combined switching and conduction loss in the SiC MOSFETs, and the conduction loss in the Schottky diodes. The Schottky diode switching loss is neglected in this exercise.

The total switching loss of the SiC MOSFETs in the CSI is estimated as [7]

$$P_{sw} = \frac{3 f_s}{\pi} (E_{on} + E_{off}) \frac{V_{llpk} I_{dc}}{V_{ref} I_{ref}} \tag{19}$$

where E_{on} and E_{off} are the turn-on and turn-off energy, respectively, at the reference voltage V_{ref} and reference current I_{ref} from the datasheet, and f_s is the PWM switching frequency. Substituting (2) into (19), the switching loss can be expressed as

$$P_{sw} = \frac{2\sqrt{3} f_s}{\pi} (E_{on} + E_{off}) \frac{V_{dc} I_{dc}}{m \cos\theta V_{ref} I_{ref}} \tag{20}$$

The conduction losses of the SiC MOSFETs and SiC Schottky diodes can be represented by the following equations

$$P_{c\_MOSFET} = 2 I_{dc}{}^2 r_{DS(on)} \tag{21}$$

$$P_{c\_diode} = 2 I_{dc} (I_{dc} r_d + V_F) \tag{22}$$

where $r_{DS(on)}$ is the drain-source on-state resistance of the SiC MOSFET, and r_d and V_F are the on-state resistance and forward voltage of the SiC Schottky diode, respectively.

The inductor loss of the CSI includes the copper loss P_{L_cu} in the winding resistance, and the core loss P_{L_fe} due to the hysteresis and eddy current losses in the magnetic core:

$$P_L = P_{L\_cu} + P_{L\_fe} \tag{23}$$

The inductor copper loss originates in the inductor winding resistance r_L, resulting in

$$P_{L\_cu} = {I_{dc}}^2 r_L \tag{24}$$

The core loss of the powered core material can be estimated in a simplified form as [13]

$$P_{L\_fe} = k {f_s}^{(i)} {B_L}^{(j)} W_{tfe} \tag{25}$$

where B_L is the peak magnetic flux density in the inductor $[T]$, W_{tfe} is the core weight $[kg]$, and k, m, n are the provided coefficients that vary with different core materials. For High Flux 60 powder cores, $k = 2.03 \times 10^{-7}$ $[\frac{s}{T \cdot kg}]$, $i = 1.23$, and $j = 2.56$.

Combining the loss components, the total CSI loss is expressed as

$$P_{CSI} = P_{sw} + P_{c\_MOSFET} + P_{c\_diode} + P_L \tag{26}$$

C. Loss Model of DC/DC Converter

The same SiC MOSFETs and SiC Schottky diodes are used to build the dc/dc converter, as shown in Fig. 1. The power loss of the dc/dc converter can be computed as

$$P_{conv} = P_{sw\_conv} + P_{c\_conv} \tag{27}$$

The switching loss of the dc/dc converter, P_{sw_conv}, at a given dc-link current I_{dc} and battery voltage V_B can be expressed as

$$P_{sw\_conv} = \frac{f_s}{\pi}\left(E_{on} + E_{off}\right)\frac{V_B I_{dc}}{V_{ref} I_{ref}} \tag{28}$$

The dc/dc converter conduction loss include SiC MOSFETs and SiC Schottky diodes can be calculated by

$$\begin{aligned} P_{c\_conv} = (1 + d_{conv}) {I_{dc}}^2 r_{DS(on)} \\ + (1 - d_{conv}) I_{dc} (I_{dc} r_d + V_F) \end{aligned} \tag{29}$$

where d_{conv} is the duty ratio of the dc/dc converter, and the relationship between the battery voltage and the average dc-link voltage at the input terminal of CSI can be expressed as [7]

$$V_{dc} = d_{conv} V_B \tag{30}$$

V. Verification of the Loss Model

The calculated losses are validated by simulation results for both the CSI and SPM machine when $m = 1$, as shown in Table II. This comparison is based on the operation point of continuous power (55 kW) at the corner speed (3,200 rpm), as shown in Table II. The battery voltage is 650 V, and the switching frequency of the dc/dc converter and CSI is 50 kHz. The simulation software MATLAB and PLECS are used to evaluate the power losses of the CSI, and JMAG is used to evaluate the motor loss. Cree 1200 V SiC MOSFETs (C3M0016120K) and 1200 V SiC Schottky diodes (C4D40120D) were selected for the CSI. To meet the current rating, three discrete SiC MOSFETs are paralleled to form a single switch, and four SiC Schottky diodes are connected in parallel for this simulation. The predicted loss from the simulation results is modestly higher than the calculated value using the formulas because of the non-ideal operation of the CSI and magnetic saturation in the machine that is incorporated into the FEA results. However, the difference in the predicted total machine drive loss between the analytical calculation and the simulation results is less than 10%.

Table II. Comparison of Total CSI Machine Drive System Loss using Analytical Calculations and Simulation

	Parameter	Calculated loss (W)	Simulation loss (W)
CSI	MOSFET switching loss	214	186.8
	MOSFET conduction loss	182	243.3
	Diode conduction loss	312	349.8
	Inductor loss	101	130
	Total CSI loss	**809**	**909.9**
Dc/dc Converter	MOSFET switching loss	86	98.4
	MOSFET and diode conduction loss	254	300.2
	Total dc/dc Converter loss	**341**	**398.6**
SPM Machine	Copper loss	2081	2070
	Core loss	150	195
	Total Machine loss	**2231**	**2265**
	Total Machine Drive loss	**3381**	**3573.5**

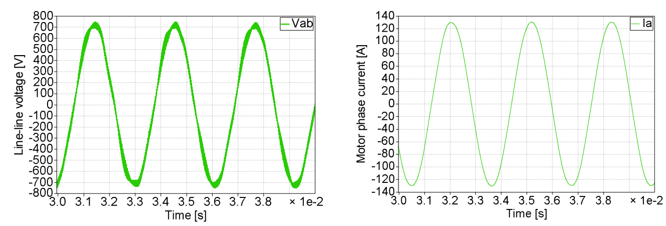

Fig. 6. Simulation results for machine line-line voltage (left) and phase current (right) @ 55kW and 3,200 rpm (corner point).

The predicted machine line-to-line voltage and phase current from the simulation are shown in Fig. 6. As noted earlier, the CSI has more sinusoidal output voltage waveforms compared to the VSI, which is beneficial for lowering the output *dv/dt* stress and common-mode EMI emissions.

VI. Drive System Efficiency Improvement Based on Genetic Algorithm Optimization

A. Impact of Modulation Index on Drive System Performance

The total losses of the drive system consisting of the dc/dc converter, CSI, and SPM machine can be calculated as

$$P_{total} = P_{motor} + P_{CSI} + P_{conv} \tag{31}$$

The operating condition chosen for this optimization exercise is 55 kW output power at the maximum machine speed

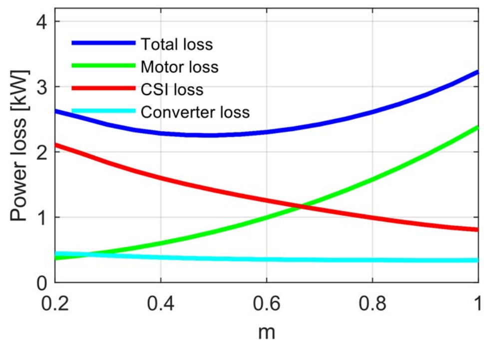

Fig. 7. Effect of modulation index m on CSI drive component losses and total drive system loss for operation at 55 kW, 20,000 rpm.

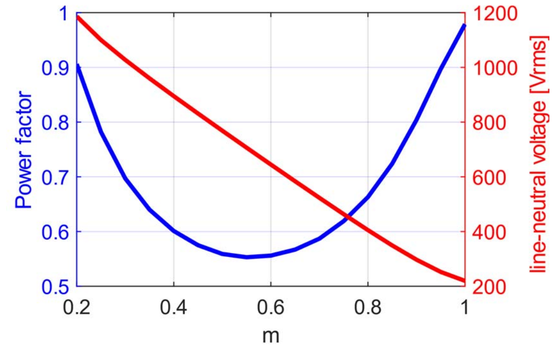

Fig. 8. Effect of modulation index m on the machine power factor and line-neutral rms voltage for operation at 55 kW, 20,000 rpm.

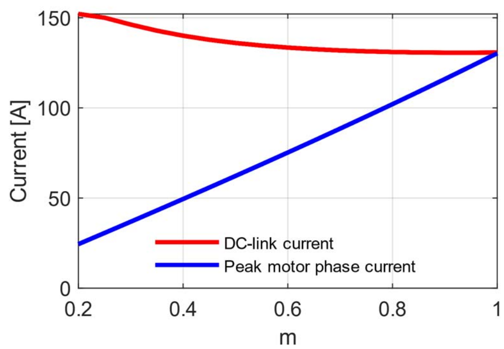

Fig. 9. Effect of modulation index m on dc-link current and peak motor phase current for operation at 55 kW, 20,000 rpm.

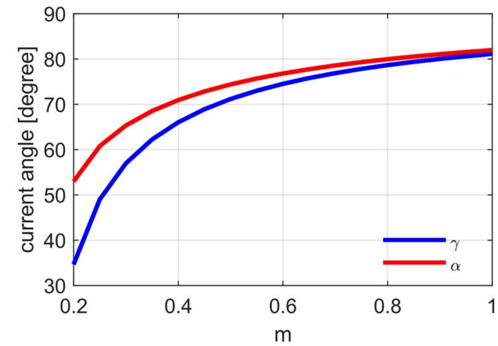

Fig. 10. Effect of modulation index m on current angle γ and angle α between CSI phase current and back-EMF for operation at 55 kW, 20,000 rpm.

of 20 krpm with 50 kHz switching frequency and 125 ℃ junction temperature for the CSI and dc/dc converter. Based on the power loss model of the dc/dc converter, CSI, and machine, the impacts of the CSI modulation index m on these three drive component losses and the total drive system loss are plotted in Fig. 7. The corresponding impact of the modulation index m on the machine power factor and the machine phase voltage are plotted in Fig. 8.

It should be noted that Figs. 7 to 10 show the predicted effect of the modulation index while ignoring the voltage ratings of the power devices. This is a simplifying assumption since the CSI boost ratio plays a major role in determining the required voltage rating of the power devices. Although this important constraint is not reflected in Figs. 7 to 10, it is considered when determining the optimal efficiency that can be achieved during constant power operation in the next sub-section.

To maintain the output power, the current angle between the current and back-EMF is also controlled as m changes. As shown in Fig. 7, decreasing m increases the CSI losses due to the direct impact of the boosted line-line voltage on the device switching loss. In contrast, the total machine loss is reduced as the modulation index m decreases because the machine phase current falls as the machine terminal voltage increases. As a result, the total machine drive power loss initially reduces as the modulation index m drops below 1, but then increases again as m is decreased below 0.5.

Fig. 8 shows the effect of modulation index m on the power factor, which exhibits the same tendency as the system loss, dipping to a minimum value in the vicinity of $m = 0.55$ and then rising again when m is reduced below that value. The line-neutral voltage increases monotonically as m is reduced. For the 1200 V SiC MOSFET and Schottky diodes that are used for this analysis, the modulation index could not be reduced below approx. 0.75 at this operation point without exceeding the voltage capability of the devices. Hence, special attention needs to be given between the rating of the device selection and voltage boost capability during design process.

Fig. 9 shows the effect of m on the dc-link current I_{dc} and motor phase current. As discussed previously, the output phase current is proportional to the modulation index m. Considering the power losses and the ac capacitor effect, the dc-link current increases modestly as m decreases. This variation of the dc-link current also affects the losses in the dc link inductor and the dc/dc converter, both of which tend to increase as m is reduced.

Fig. 10 shows the effect of m on the current angle γ between back-EMF and stator current and α between the back-EMF of the motor and CSI output current before the capacitor. Their downward trends as m is reduced confirm that operating the motor at a higher terminal voltage makes it possible to reduce the negative d-axis current amplitude during flux-weakening operation. It should be noted that at this operation point (55 kW, 20 krpm), the stator current of the motor is leading the phase voltage because the machine is over-excited. This means that the ac capacitor has a negative effect on the power factor by adding an additional leading angle to the current so that α is larger than γ, as shown in Fig. 10.

B. Multi-Objective Optimization of CSI Modulation Index

Due to the complex loss model of CSI and motor, as well as the nonlinearity of the power factor, the determination of the optimum modulation index and the angle between stator current and back EMF is a complicated and multi-variable problem. Hence, a multi-objective optimization using a genetic algorithm has been adopted to investigate the opportunities for improved performance in the constant-power region [14]. This optimization is carried out based on the analytical equations derived for the CSI drive system operation in (1) to (12) and the loss equations in (13) to (30).

In this optimization, the free variables are the CSI modulation index (m) and the current angle between stator current and back EMF (γ). The objective variables that are being optimized are minimization of the drive system loss (equivalent to maximized drive efficiency) and maximization of the power factor. The population size and generations for the genetic algorithm are set as 1,000 and 10,000, respectively. The solutions are limited to those resulting in a peak line-line voltage less than 1000 V to respect the 1200 V rating of the power switches.

The flowchart of the proposed methodology is shown in Fig. 11. First, the initial population is created with a set of 1,000 designs or "individuals" (i.e., 1,000 sets of input variables) and the constraints are determined based on the machine parameters and performance metrics. Then the objectives of this population are evaluated, and the Pareto front is determined so that no other design in this population dominates the designs along the Pareto front. The new generation population is created with the best designs from the old generation and a percentage of exploratory

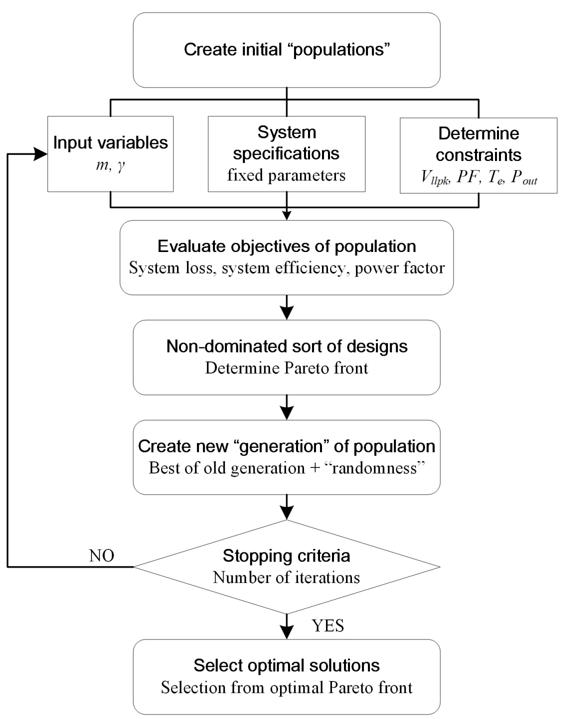

Fig. 11. Flowchart of the genetic algorithm optimization to improve the drive system efficiency using the CSI's voltage boost function.

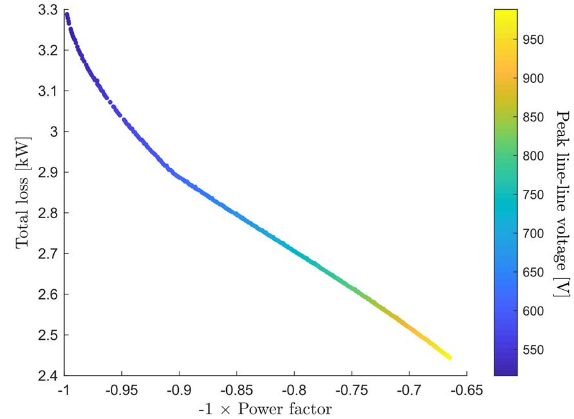

Fig. 12. Pareto front showing trade-offs between total drive losses and power factor by varying modulation index for operation at 55 kW, 20,000 rpm.

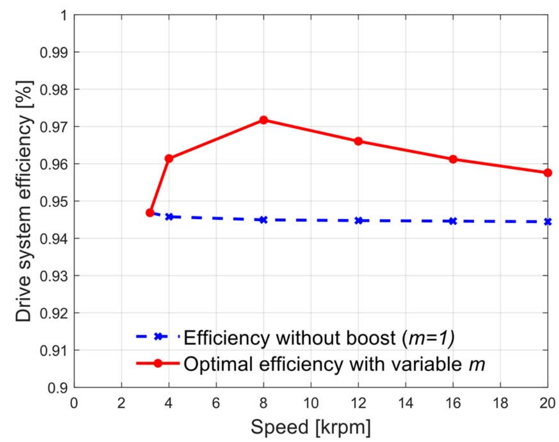

Fig. 13. Comparison of the CSI drive system efficiency along envelope in the constant-power region with and without CSI's voltage boost function.

designs that use random number generators to select the input variables. After 10,000 iterations, the optimal solutions can be selected from the Pareto front.

The Pareto-optimal front of the final generation is shown in Fig. 12 for the same 20,000 rpm, 55 kW operating point in deep flux weakening investigated earlier in this section. The x-axis is the power factor (with a negative sign so that its "best" value is at the left end of the axis); the y-axis is the total drive system loss, and the marker fill color is the peak line-line voltage. The points in the Pareto front consists of the set of Pareto optimal solutions which are not dominated by any other solution. This plot facilitates the trade-off decision between the total drive system loss and the power factor. Because of the voltage limit of the power switches which is the constraint in the optimization, the optimal modulation index cannot be lower than 0.65, as shown in Fig. 12. In this investigation, system efficiency is the prime objective, so the lowest system loss design is selected.

In order to evaluate the efficiency improvement that is available by varying the modulation index, the maximum efficiency of the complete CSI drive system with ($m \leq 1$) and without ($m = 1$) voltage boost are compared during operation along the envelope in the constant-power region, as shown in

TABLE III. DRIVE SYSTEM EFFICIENCY IN CONSTANT-POWER REGION WITH FIXED AND OPTIMIZED MODULATION INDEX VALUES

Speed [rpm]	*m*	γ [degree]	Peak line-line voltage [V]	Power factor	Drive Sys. Effic. [%]
Original modulation index (m = 1)					
3,200	1	0	710.9	0.785	94.68
4,000	1	38.66	568.6	0.926	94.57
8,000	1	67.28	527.9	0.997	94.49
12,000	1	75.10	527.7	0.999	94.47
16,000	1	78.84	531.3	0.989	94.46
20,000	1	81.13	538.0	0.979	94.44
Optimal modulation index and current angle					
3,200	1	0	710.9	0.785	94.68
4,000	0.845	12.80	803.2	0.812	96.14
8,000	0.565	41.60	985.8	0.978	97.17
12,000	0.683	65.98	979.5	0.807	96.60
16,000	0.775	74.49	995.5	0.712	96.12
20,000	0.835	78.63	996.0	0.662	95.75

Fig. 13. It can be observed that the optimal system efficiency can be increased roughly 1% to 2.5% by utilizing the boost function of the CSI in field weakening region. This is an important observation for the capability and optimization of the CSI for traction applications with large CSPR.

The optimum modulation index *m* and several key drive system variables corresponding to the envelope operating points in the constant-power region plotted in Fig. 13 are provided in TABLE III. As the boost function of CSI is utilized, a lower current angle γ is needed during flux-weakening operation. Even though the power factor is reduced as the modulation index *m* decreases, the system efficiency is significantly boosted which is a high priority for traction drive applications.

All of the operating points with variable modulation index values have peak line-line voltages less than 1000 V as noted above. As manufacturers of WBG power devices develop new generations of devices with higher voltage ratings and better performance, the CSI's voltage boost function will become increasingly valuable for raising the drive system efficiency.

VII. CONCLUSION

This paper investigates the effect of the CSI's voltage boost function on CSI drive system efficiency improvement in the constant-power operating regime. The *dq* model of the CSI-based machine including the impact of the ac capacitors has been developed to reduce the modeling error in the high-speed regime. Analytical equations for the operation of the SPM machine, CSI, and the dc/dc converter have been derived, including loss models for all of the key components.

Using these analytical equations, the effects of the CSI's modulation index on the total drive system efficiency and power factor have been investigated. A genetic algorithm has been used to identify the optimal modulation index and current angle along the envelope of the constant power region. It has been shown that the optimal drive system efficiency when using the boost function while respecting the maximum voltage ratings of the WBG switches is between 1% and 2.5% higher than the efficiency without voltage boost. As a result, the CSI's voltage boost function opens valuable opportunities to improve the traction drive system efficiency during high-speed operation.

ACKNOWLEDGMENT

This material is based on work supported by the U.S. Department of Energy's Office of Energy Efficiency and Renewable Energy (EERE) under the Vehicle Technologies Office (VTO), Award Number DE-EE0008704. The authors also gratefully acknowledge the support of the Wisconsin Electric Machines and Power Electronics Consortium (WEMPEC).

REFERENCES

[1] M. Yilmaz and P. T. Krein, "Review of battery charger topologies, charging power levels, and infrastructure for plug-in electric and hybrid vehicles," in *IEEE Transactions on Power Electronics*, vol. 28, no. 5, pp. 2151-2169, May 2013.

[2] X. Ding, H. Guo, R. Xiong, F. Chen, D. Zhang, and C. Gerada, "A new strategy of efficiency enhancement for traction systems in electric vehicles," in *Applied Energy*, vol. 205, pp. 880-891, Nov. 2017.

[3] X. Ding, G. Liu, M. Du, H. Guo, C. Duan, and H. Qian, "Efficiency improvement of overall PMSM-inverter system based on artificial bee colony algorithm under full power range," in *IEEE Transactions on Magnetics*, vol. 52, no. 7, pp. 1-4, July 2016.

[4] G. Su and L. Tang, "Current source inverter based traction drive for EV battery charging applications," in *Proc. 2011 IEEE Vehicle Power and Propulsion Conference*, Chicago, IL, 2011, pp. 1-6.

[5] H. Dai, T. M. Jahns, R. A. Torres, D. Han, and B. Sarlioglu, "Comparative evaluation of conducted common-mode EMI in voltage-source and current-source inverters using wide-bandgap switches," in *Proc. IEEE Transportation Electrification Conference and Expo (ITEC)*, Long Beach, CA, 2018, pp. 788-794.

[6] R. A. Torres, H. Dai, W. Lee, T. M. Jahns, and B. Sarlioglu, "Current-source inverters for integrated motor drives using wide-bandgap power switches," in *Proc. IEEE Transportation Electrification Conference and Expo (ITEC)*, Long Beach, CA, 2018, pp. 1002-1008.

[7] G. Su and P. Ning, "Loss modeling and comparison of VSI and RB-IGBT based CSI in traction drive applications," in *Proc. IEEE Transportation Electrification Conference and Expo (ITEC),* Detroit, MI, 2013, pp. 1-7.

[8] G. Su, L. Tang, and Z. Wu, "Extended constant-torque and constant-power speed range control of permanent magnet machine using a current source inverter," in *Proc. IEEE Vehicle Power and Propulsion Conference*, Dearborn, MI, 2009, pp. 109-115.

[9] L. Tang and G. Su, "Boost mode test of a current-source-inverter-fed permanent magnet synchronous motor drive for automotive applications," in *Proc. IEEE 12th Workshop on Control and Modeling for Power Electronics (COMPEL),* Boulder, CO, 2010, pp. 1-8.

[10] M. N. Uddin and R. S. Rebeiro, "Online efficiency optimization of a fuzzy-logic-controller-based IPMSM drive," in *IEEE Transactions on Industry Applications*, vol. 47, no. 2, pp. 1043-1050, March-April 2011.

[11] S. Vaez, V. I. John and M. A. Rahman, "An on-line loss minimization controller for interior permanent magnet motor drives," in *IEEE Trans. on Energy Conversion*, vol. 14, no. 4, pp. 1435-1440, Dec. 1999.

[12] M. Liu, W. Sixel, Y. Li, J. Tangudu, V. Blasko and B. Sarlioglu, "Design and comparison of single-layer dual-stator 6/4 FSPM machine with toroidal winding," in *Proc. IEEE Energy Conversion Congress and Exposition (ECCE)*, Baltimore, MD, USA, 2019, pp. 3813-3819.

[13] Wm. T. McLyman, Transformer and inductor design handbook, 3rd ed., Marcel Dekker, Inc., 2004, pp. 72-76.

[14] Scott D. Sudhoff, Power Magnetic Devices: A Multi-Objective Design Approach, John Wiley & Sons, Inc., Hoboken, New Jersey, 2014.